Review

A Short Review on the Corrosion Behaviour of Wire and Arc Additive Manufactured Materials

Davi Alves Marques [ID], João Pedro Oliveira *[ID] and Ana Catarina Baptista *[ID]

CENIMAT/I3N, Department of Materials Science, NOVA School of Science and Technology, Universidade NOVA de Lisboa, 2829-516 Caparica, Portugal
* Correspondence: jp.oliveira@fct.unl.pt (J.P.O.); anacbaptista@fct.unl.pt (A.C.B.)

Abstract: Wire and Arc Additive Manufacturing (WAAM) is a deposition rate process for the creation and/or repair of large structural metallic components. The non-equilibrium heating and cooling conditions associated with WAAM lead to the development of heterogenous microstructures. Although there is a large body of work focusing on the microstructure and mechanical properties of WAAM-fabricated components, assessment of the corrosion behaviour of alloys fabricated by WAAM is still in its infancy. In this review, the current body of knowledge associated with the corrosion behaviour of different WAAM-fabricated engineering alloys is presented and discussed. Future perspectives and potential research topics are also presented. This is the first review work focusing on the corrosion of wire and arc additive manufactured materials.

Keywords: wire and arc additive manufacturing; corrosion; microstructure

1. Introduction

Metallic materials are part of day-to-day life as they are key in the improvement of living conditions around the world. Conventional manufacturing processes for metallic materials allow to create multiple components, but often there are design limitations imposed by the manufacturing process itself. The advent of additive manufacturing (AM) allowed for complex-shaped structures to be easily fabricated in a layer-by-layer fashion and for the construction of complex geometries with satisfactory accuracy [1]. Although AM processes can be applied to any class of engineering materials [2–5], metal additive manufacturing is currently expanding given the potential applicability prospects associated with the combination of high strength metallic alloys with improved design flexibility enabled by AM processes. Although most AM processes for metallic materials are focused on the fabrication of small- to medium-sized components, there is a significant and urgent need for processes capable of fabricating larger complex-shaped structures in a timely fashion, while decreasing material waste. With regards to this, within the field of metal additive manufacturing, wire and arc additive manufacturing (WAAM) has a large deposition rate and is known for its low implementation costs and easy maintenance [6]. WAAM is already being used in the industry field for multiple applications, ranging from the repair of obsolete metallic components to the fabrication of new parts, as well as in the oil and gas, energy and aerospace industries [7–10]. In WAAM, the large heat source can be based on gas metal arc welding (GMAW) [11–15], gas tungsten arc welding (GTAW) [16–19], or plasma arc welding (PAW) [20–24]. The selection of each of these types of heat sources will influence the microstructure development, process stability, deposition rate, implementation costs and industrial uptake.

Currently, WAAM of different engineering alloys is primarily focused on determining the evolution of microstructure and the resulting mechanical properties [25–31]. Determining the relationships between microstructure and mechanical properties is currently fundamental since the application prospects of WAAM-fabricated components is for them to be used in structural applications. Hence, it is necessary that how the weld thermal

cycle impacts the microstructure along the deposited material is understood so that one can develop new processing conditions or post-process heat treatments, targeting an improvement in the resulting mechanical properties. Despite the importance of linking processing conditions to microstructure and mechanical response, there are other key material features that must be comprehensively assessed to further expand the use of WAAM in key industry sectors where the materials are in contact with aggressive environments, such as in the oil and gas and nuclear industries [28,32]. A key topic that has been lacking attention, with scarce literature to be found on it, is the assessment of the corrosion behaviour of WAAM-fabricated components. There is a fundamental need to address the corrosion behaviour of components built by WAAM as the type of applications associated with this technology, namely large metallic components for critical application in the oil and gas, maritime and aerospace industries, often require that the components be used in demanding, aggressive environments. More importantly, it is well-known that the thermal conditions within a part fabricated by WAAM are dependent on the location of the part. Since there is often a correlation between the thermal cycle experienced by the material and the resulting microstructure (coming from the solidification structure or due to solid state transformations imposed by repeated subsequent depositions), the thermophysical properties, including corrosion behaviour of the fabricated component, can be spatially dependent, which can aggravate the deterioration of the structural integrity during the operation of the component.

The present review work focuses on the current state of the art for the assessment of the corrosion behaviour of different alloy families fabricated by WAAM. We highlight key features associated with each type of material, while also suggesting new venues for research so that WAAM can be fully embraced and adopted at an industrial level in high-demand applications.

2. Methodology

The present review was conducted by searching articles from the scientific platforms Scopus, ScienceDirect and Google Scholar using "wire arc additive manufacturing", "WAAM", "corrosion behaviour" and "corrosion" as key words. Multiple combinations of these keywords were used to ensure that all the articles related to the corrosion of WAAM-fabricated materials were considered. The articles were then sorted by the type of alloys, as it will be mentioned in the study, and a second search was made including the different base metals as key words, i.e., "steel", "stainless steel", "nickel", "titanium" and "magnesium", as a second-step method to guarantee the effectiveness of the search. The articles were analysed to filter the ones that only mentioned corrosion in a brief and undetailed manner, those that focused mostly on mechanical properties and those that focused on the corrosion behaviour with more details. After the filtering process, the remaining papers were used to compose the present review work.

It is worth mentioning that several of these scientific studies were conducted as a mixture of corrosion and mechanical properties analysis, and for this reason did not utilise the full spectrum of electrochemical analysis techniques possible.

3. Corrosion Behaviour in WAAM Materials

Corrosion is defined as a spontaneous reaction that results in material degradation as a result of its interaction with the environment [33]. The material's susceptibility to corrosion is a parameter that depends on different factors, including the corrosive environment, the chemical composition of the material, heat treatment, microstructure, surface finish, production and processing methods [34,35].

When addressing wire arc additive manufactured (WAAMed) materials, some of the process parameters, such as travel speed, wire feed rate, current, deposition path and protection gas flow rate [36,37], significantly affect the resulting microstructure and surface finish and, thus, will have an observable impact on the corrosion behaviour, as previously mentioned. This multiple-parameter effect leads to difficulty in determining their isolated

influence. Despite this issue, some authors suggested that a synchronous effect can be condensed and analysed in terms of heat input [38,39].

Compared to conventionally produced methods, AM components present complex microstructures because of the different time-dependent temperature profiles and process parameters [40–48]. These microstructures are formed by a combination of rapid solidification rates and high thermal gradients [49]. These processes are known to produce complex, non-equilibrium microstructures with poor surface finish, resulting in the necessity of post-processing treatments. Dinovitzer et al. [38] reported an increase in surface roughness with higher travel speeds and presented an inverse behaviour relative to the current applied during the WAAM process, leading to an increase in corrosion susceptibility [50,51].

Another important factor inherent to this process is the segregation of alloying elements, which is a result of different concentrations and solidification times of the dendritic and interdendritic regions, leading to chemical heterogeneities creating large cathodic regions enabling localised corrosion [52,53]. Figure 1 displays the microstructure comparison between conventionally produced and AMed steels. The adjustment of the operating parameters allows the control of the cooling rates during and after solidification, which results in tunning of the microstructure, leading to higher strength without significantly reducing the ductility.
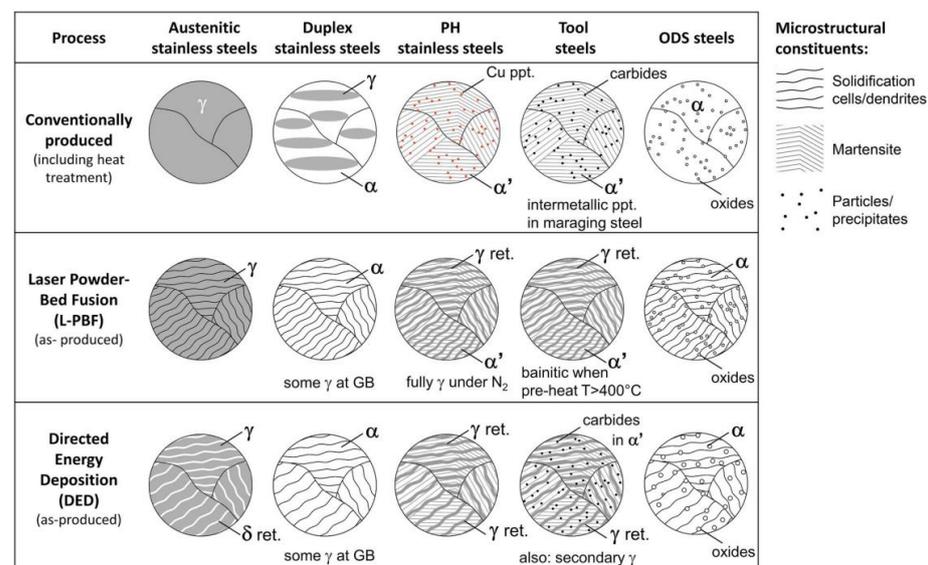
Figure 1. Typical microstructures of different steels produced conventionally (in the state intended for use) and after additive manufacturing. Reprinted with permission from [53].

Despite the increasing attention WAAMed materials are attracting, there is still a lack of information in the literature concerning its corrosion behaviour [54–56], which is of fundamental importance prior to a massive industrial application of these materials into industrially relevant settings. Figure 2 details the growing trend in WAAM corrosion studies, which total approximately 560 papers published during the period from 2018 to 2022. During the same period, Laser Power-Bed Fusion (L-PBF) corrosion presented twice as much research works [57]. Despite the increase in the number of papers, these studies focus on specific topics related to a particular problem and/or application rather than seek a general comprehension of the corrosion susceptibility [8,25,28,58–66]. The following sections summarise the key knowledge associated with the corrosion behaviour of different material classes fabricated by WAAM.
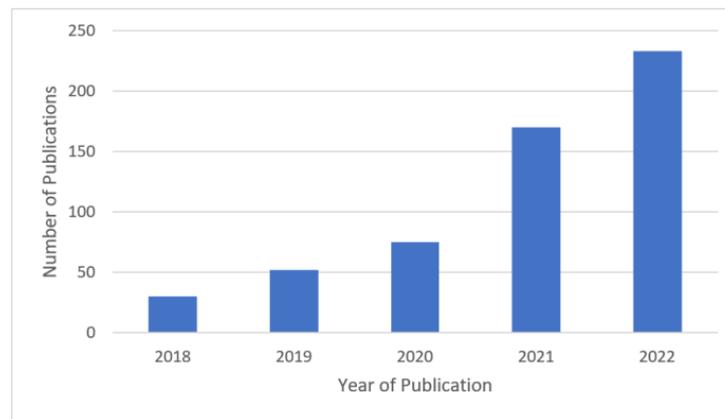
Figure 2. The number of publications related to corrosion in WAAM materials (data extracted from ScienceDirect® [57]).

3.1. Steels

Tian et al. [67] studied the galvanic corrosion of a low-carbon high-strength steel 10CrNi3MoV fabricated by cold metal transfer (CMT) WAAM in a 3.5% NaCl solution comparing the substrate with the deposited layers. Optical microscope imaging taken after 1 h of immersion showed a more severe pitting and overall corrosion in the deposited layers when compared to the substrate. This contrast was more evident after 12 h of immersion where the deposited layer presented a large number of oxides and pitting corrosion and the substrate presented fewer corrosion products, as seen in Figures 3 and 4 [67]. The difference in corrosion resistance was attributed to high process heat input and an uneven microstructure, resulting in differences in both grain size and element segregation causing micro-galvanic corrosion [67]. This work elucidated the importance of process control to produce compatible microstructures aiming to reduce differences in electrochemical properties and, thus, improve their functionality.
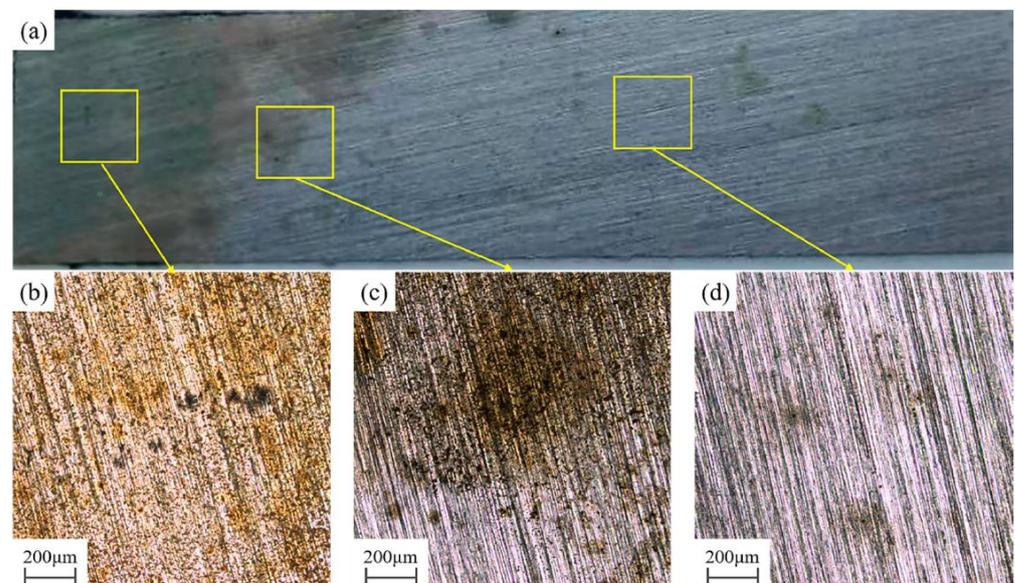
Figure 3. Morphologies after 1 h of immersion in 3.5% NaCl solution: (**a**) macroscopic image of the deposited layer; (**b**) optical microscope of the substrate; (**c**) optical microscope image of the junction; (**d**) optical microscope image of the matrix. Reprinted with permission from [67].
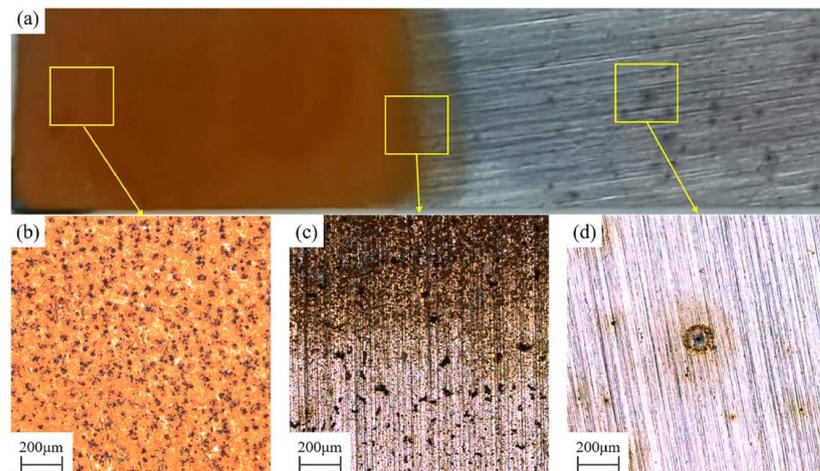
Figure 4. Morphologies after 12 h of immersion in 3.5% NaCl solution: (**a**) macroscopic image of the deposited layer; (**b**) optical microscope image of the substrate; (**c**) optical microscope image of the junction; (**d**) optical microscope image of the matrix. Reprinted with permission from [67].

Ron et al. studied the corrosion behaviour of WAAMed ER70S-6 compared to the reference alloy ST-37 in a 3.5% NaCl solution [68]. The results obtained by potentiodynamic polarisation, and electrochemical impedance spectroscopy (EIS) showed that the electrochemical behaviour of both printed and reference alloys was practically the same and presented comparable corrosion rates. Despite the similarity of both specimens, the corrosion degradation mechanisms were different. ER70S-6 presented uniform exfoliation corrosion, while the reference alloy presented localised corrosion resulting in the formation of a porous area, as seen in Figure 5. The difference in corrosion mechanisms was attributed to variations in chemical composition as a result of different solidification rates, creating a more homogenous microstructure and reduced amounts of secondary pearlite phase for the printed alloy. Due to the slower solidification, the reference alloy presented larger quantities of pearlite, resulting in micro-galvanic corrosion [68].
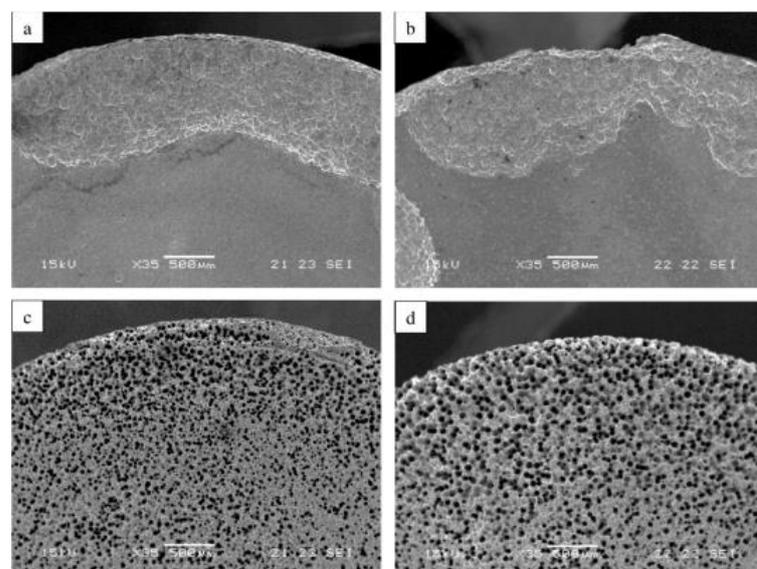
Figure 5. SEM imaging of the surface morphology after immersion tests in 3.5% NaCl solution: (**a**,**b**) WAAMed alloy after exposure of 60 and 90 days, respectively; (**c**,**d**) reference alloy after exposure of 60 and 90 days, respectively. Reprinted with permission from [68].

3.2. Stainless Steels

Wen et al. [69] observed that high linear heat input (LHI) during WAAM of austenitic stainless steel provided a larger molten region and lower cooling rates enabling a longer diffusion time for atoms such as Cr and Mo, thus, resulting in the segregation of these species. The final microstructure presented austenitic and δ-ferrite regions composed of Cr/Mo-poor and high LHI, with Cr/Mo-rich and low LHI passive films, respectively, favouring the localised corrosion as a result of the formation of a galvanic cell. The polarisation curves, operated in a 3.5 wt% NaCl solution, show that despite both WAAMed steels presenting lower corrosion potential than the wrought, the specimen produced using low LHI displayed a higher pitting potential and a larger passivation voltage range (the difference between corrosion and pitting potential), as seen in Figure 6, which is an indication of a stable passive film formation [70,71].
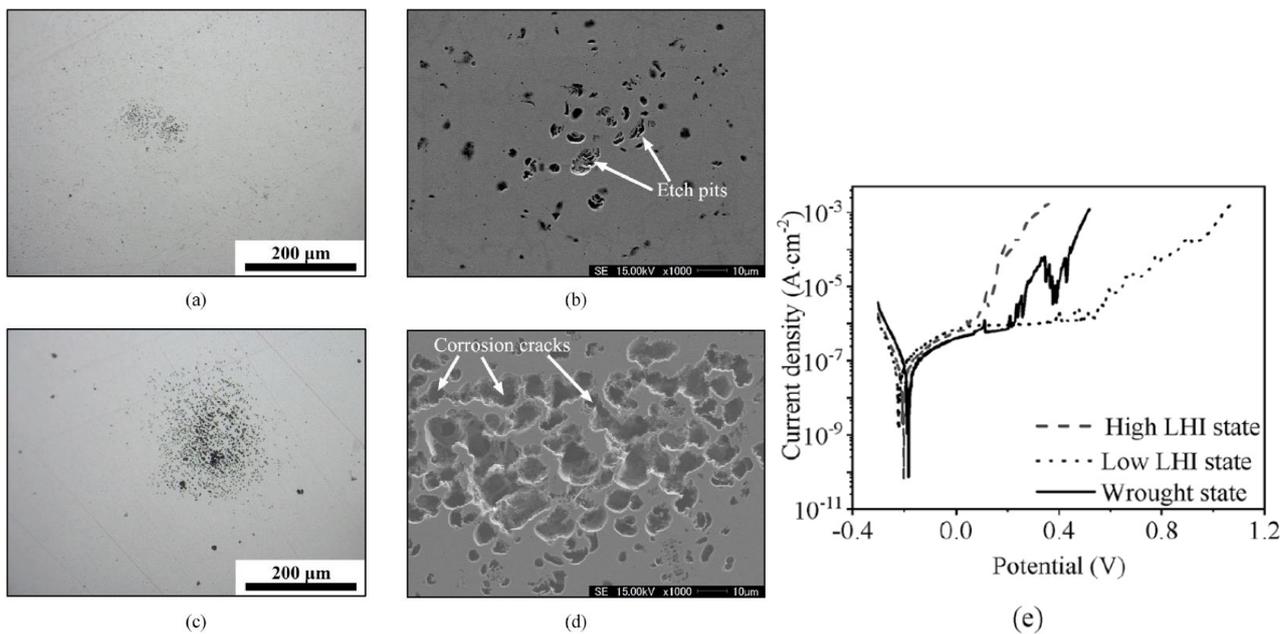

Figure 6. Morphology of pitting corrosion under (**a**,**b**) low LHI; (**c**,**d**) high LHI and (**e**) corresponding electrochemical polarisation curves. Reprinted with permission from [69].

Hao et al. [72] prepared samples of SUS304 via WAAM and studied the corrosion behaviour in 3.5% NaCl solution as a function of the applied current by comparing the constant current (CC) of 150 A with a 2 Hz pulse current (PC) composed of a base current of 150 A, a peak current of 200 A and a 0.2 m/min travel speed. They noticed that the specimens produced with PC presented more positive corrosion potentials, indicating a lower corrosion rate. This finding was attributed to the higher relative content of Cr and Ni in the layers deposited with PC.

The investigation of pitting corrosion resistance of super duplex stainless steel (ER2594) fabricated by WAAM was analysed in three different regions, the bottom, middle and top of the deposited wall in a 3.5% NaCl solution [73]. It was found that the position of the deposited material had little to no effect on the corrosion resistance. The corrosion rates extracted using the Tafel curves resulted in excellent resistance [74] and were comparable to that of the wrought alloy. The Pitting Resistance Equivalent Number (PREN) of all the regions presented results higher than 40, indicating that it is suitable for oil and gas industry applications, as required by the National Association of Corrosion Engineers (NACE) [75] and suitable for seal rings in subsea connections, as required by the Norwegian shelf's competitive position (NORSOK) [76].

3.3. Nickel Alloys

Zhang and Ojo [77] studied the corrosion behaviour of WAAMed Inconel 718 (IN718) in 1 M nitric acid (HNO$_3$) and in 1 M sulfuric acid (H$_2$SO$_4$) using the wrought alloy as a benchmark. Despite both alloys receiving the same post-manufacturing heat treatment, the WAAMed alloy had higher corrosion current density (i$_{corr}$), passivation current density (i$_{pass}$), critical current density (maximum density of active–passive transition, i$_{crit}$) and a narrower passivation potential range (ΔEpass) in both solutions, as shown in Figure 7. The higher i$_{pass}$, the more difficult the formation of a passive film is [78], hindering the corrosion resistance. Additionally relative to the passive film, wider ΔEpass indicates a more stable passive film has been formed.
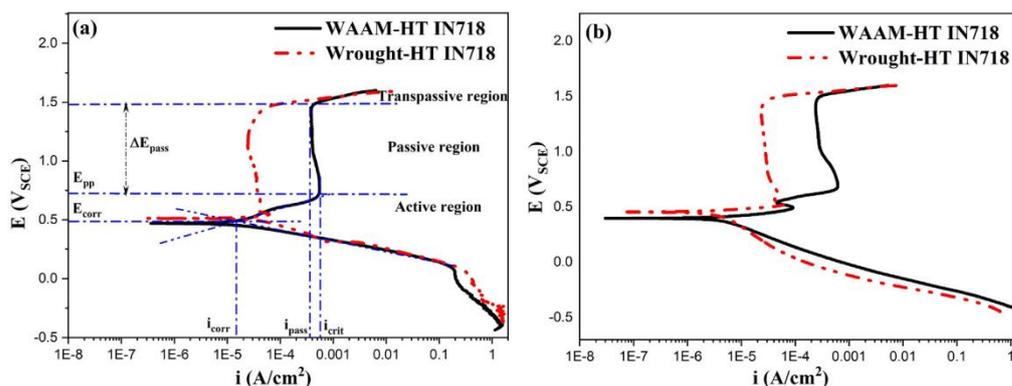

Figure 7. Potentiodynamic polarisation curves of WAAMed IN718 and Wrought IN718 at room temperature in (**a**) 1 M HNO$_3$ and (**b**) H$_2$SO$_4$ solutions. Reprinted with permission from [77].

The EIS measurements presented a considerably smaller capacitive arc in the Nyquist plots for the WAAMed IN718, indicating a lower corrosion resistance, as seen in Figure 8a, which is in accordance with the polarisation results. Although the *Y*-axis of the Nyquist plot presents the imaginary part of the impedance as positive values, the correct form to represent is with negative values. The analysis of the Bode diagrams, Figure 8b,c, showed lower values of polarisation resistance and the value of |Z| at low frequencies (f < 1 Hz) for the WAAMed IN718, which is an indication of a less stable passive film. Finally, the lower phase angle at low frequencies, seen in the WAAMed IN718, suggests a passive film with lower protection capabilities. These differences were attributed to the chemical structure of the WAAMed IN718 passive film, which contains less Cr$_2$O$_3$ and more NiO, resulting in a more porous and less protective passive film [77].
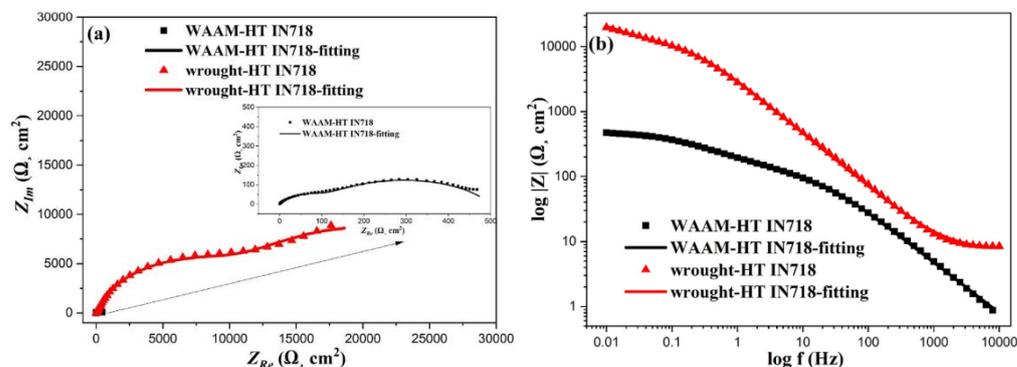
Figure 8. *Cont.*
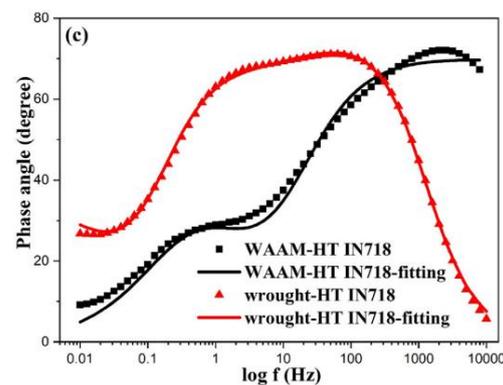
Figure 8. Electrochemical impedance spectroscopy (EIS) of WAAMed IN718 and wrought IN718 in 1 M H_2SO_4 solution after potentiostatic polarization at 1 V for 1 h at room temperature: (**a**) Nyquist plots, (**b**) Bode diagram—impedance, (**c**) Bode diagram—phase angle. Reprinted with permission from [77].

Chigilipalli and Veeramani [79] compared the corrosion behaviour of WAAMed and wrought 825 alloys in 3.5% NaCl solution and observed that the WAAMed alloy presented similar corrosion potential (E_{corr}) to the wrought alloy, −346 mV and −331 mV, respectively, and presented i_{corr} one order of magnitude higher, resulting in a corrosion rate of 0.117 mmpy, while the wrought 825 presented 0.066 mmpy. The higher density of grain boundaries present in the WAAMed alloy, when exposed to the corrosive media, can be responsible for the reduction in the corrosion resistance [80]. In addition, the decreased dislocation density of the wrought alloy increased the corrosion resistance [81].

The EIS results displayed a lower impedance value, approximately one order of magnitude for the WAAMed, which is an indication of lower corrosion resistance [82]. The phase angle at medium frequencies is associated with the integrity of the passive film, and the lower values observed for the WAAMed alloy indicates a less stable passive film with lower protection capabilities.

The lower corrosion resistance of the WAAMed alloy was associated with finer grain size and increased dislocation density. These results are in accordance with those previously observed by Zhang and Ojo [77].

3.4. Other Materials

This section is reserved to present information on other important engineering alloys that present less scientific research on the corrosion behaviour of their WAAMed specimens.

3.4.1. Titanium Alloys

Yang et al. [83] studied the corrosion behaviour of the Ti-6Al-4V alloy produced by different additive manufacturing techniques and compared it to traditional rolling in a 3.5 wt% NaCl solution. The results derived from potentiodynamic polarisation showed that the WAAMed and rolled alloys exhibited i_{corr} values nearly two orders of magnitude lower than the SLM sample, presenting approximately 0.55, 0.49 and 7.74 $\mu A/cm^2$, respectively. The corrosion rate of each specimen was calculated applying the corrosion current densities in Faraday's law [84]. The WAAMed and rolled alloys presented similar values, 4.76×10^{-3} and 4.24×10^{-3} mm/year, while the SLM presented 6.70×10^{-2} mm/year. These results indicate that WAAMed and rolled titanium alloys are classified as very stable, while SLM is classified as stable in the 3.5 wt% NaCl solution, according to Yang et al. [83]. Further investigations were conducted using the EIS and electrochemical equivalent circuit (EEC) techniques. The literature states that titanium alloys produce a duplex passivation oxide composed of an inner compact thin layer and an outer porous external layer [85,86]. The authors noted that the Bode plot shows a broad peak, which indicates the occurrence of more than one simultaneous process and can be represented by two time-cons [1]. This structure can be simulated using the EEC consisting of a solution resistance (R_s), charge

transfer resistance (R_{ct}), film resistance (R_1) and constant phase elements (CPE) representing the capacitance of the film/oxide layer interface (Q_{dl}) and the coating capacitance (Q_1), as seen in Figure 9.
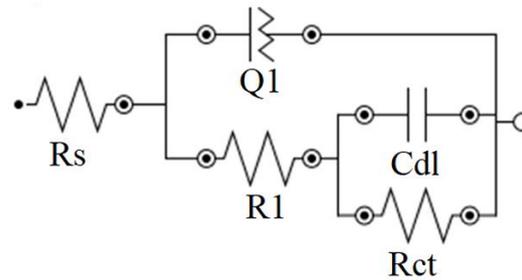
Figure 9. Electrochemical Equivalent Circuit used for modelling Ti-6Al-4V. Elaborated by author using the software Nova 2.1.

The resistance of the passive film for the WAAMed and SLM were similar and presented one order of magnitude lower than the rolled sample; 1.49, 1.56 and 21.36 kΩ cm^2, respectively. Despite this difference in the film resistance, the charge transfer resistance of the WAAMed and rolled alloys presented as one order of magnitude higher than the SLM; 49.89, 56.99, and 1.16 kΩ cm^2, respectively, indicating that both passive films present similar corrosion resistance [83]. These results are in accordance with the results obtained by the potentiodynamic tests.

The CPE's represent non-ideal capacitors, or pseudo-capacitors, represented by $Z_{CPE} = Q^{-1}(j\omega)^{-n}$, with n presenting values between 0 and 1. If the value of n is 0, the element behaves as an ideal resistance and if the value is 1 it behaves as an ideal capacitor. Typical values for n in corrosion systems are between 0.7 and 0.9, and these elements are used to substitute ideal capacitors due to the non-uniformities of the surface, i.e., heterogeneous properties and structural defects [87].

The n-values associated with coating capacitance for the WAAMed, SLM and rolled samples were 0.92, 0.85 and 0.75, respectively, and are in accordance with the Bode plot obtained. Pan et al. [87] related the presence of two time-constants to the integrity of the passive film along with the analysis of the phase angle of the Bode diagram. The medium frequency range of the diagram indicates the condition of the film's corrosion resistance; angles near $-90°$ indicate a well-formed film with good corrosion resistance. In the Bode diagram, the angles for the WAAMed, SLM and rolled alloys are approximately $-80°$, $-72°$ and $-66°$, respectively, suggesting that the WAAMed structure presents better passive film properties.

The authors concluded that the corrosion behaviour of the Ti-6Al-4V alloys was dependent on a combination of factors, including microstructure type, size and morphology of constituent phases. The WAAMed and rolled samples presented comparable corrosion resistance and were superior to the SLM. It was also noticed that the SLM sample significantly improved the corrosion resistance after the application of a proper heat treatment to induce the transformation of acicular α' martensite into a fine lamellar structure composed of α and β phases. This higher corrosion resistance of the heat treated SLM may be attributed to the finer grain structure of the material and is explained by the adherence of the passive film to the interface of the grain boundaries due to pinning effect [83], thus, reducing the material pitting corrosion susceptibility.

In a similar study, Wu et al. [88] investigated the anisotropic behaviour of WAAMed Ti-6Al-4V in 3.5% NaCl solution comparing the base metal (BM), horizontal plane (HP) and vertical plane (VP), as seen in Figure 10. As the layers build up, the cooling rate decreases, leading to a variation in the component microstructure. The BM presents an equiaxed α/β microstructure while the WAAMed presents an inhomogeneous microstructure composed of acicular martensite α' and fully lamellar α for the HP and VP.
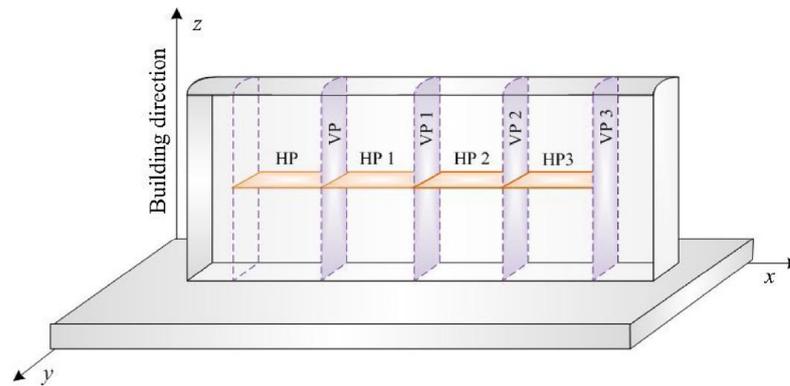
Figure 10. Three-dimensional diagram of WAAM-fabricated Ti-6Al-4V wall showing orientation of specimen planes. Reprinted with permission from [88].

The electrochemical properties were analysed via potentiodynamic polarisation and EIS, showing that the anisotropic behaviour affected the corrosion properties. The HP plane presented higher i_{pass}, suggesting higher corrosion rates. Although the Nyquist and Bode plots appear similar for all the specimens, the simulation using a Randles circuit showed that the BM presented R_f values one order of magnitude higher than the VP and HP regions, as seen in Figures 11 and 12. These findings are in accordance with the study of Yang et al. [83].
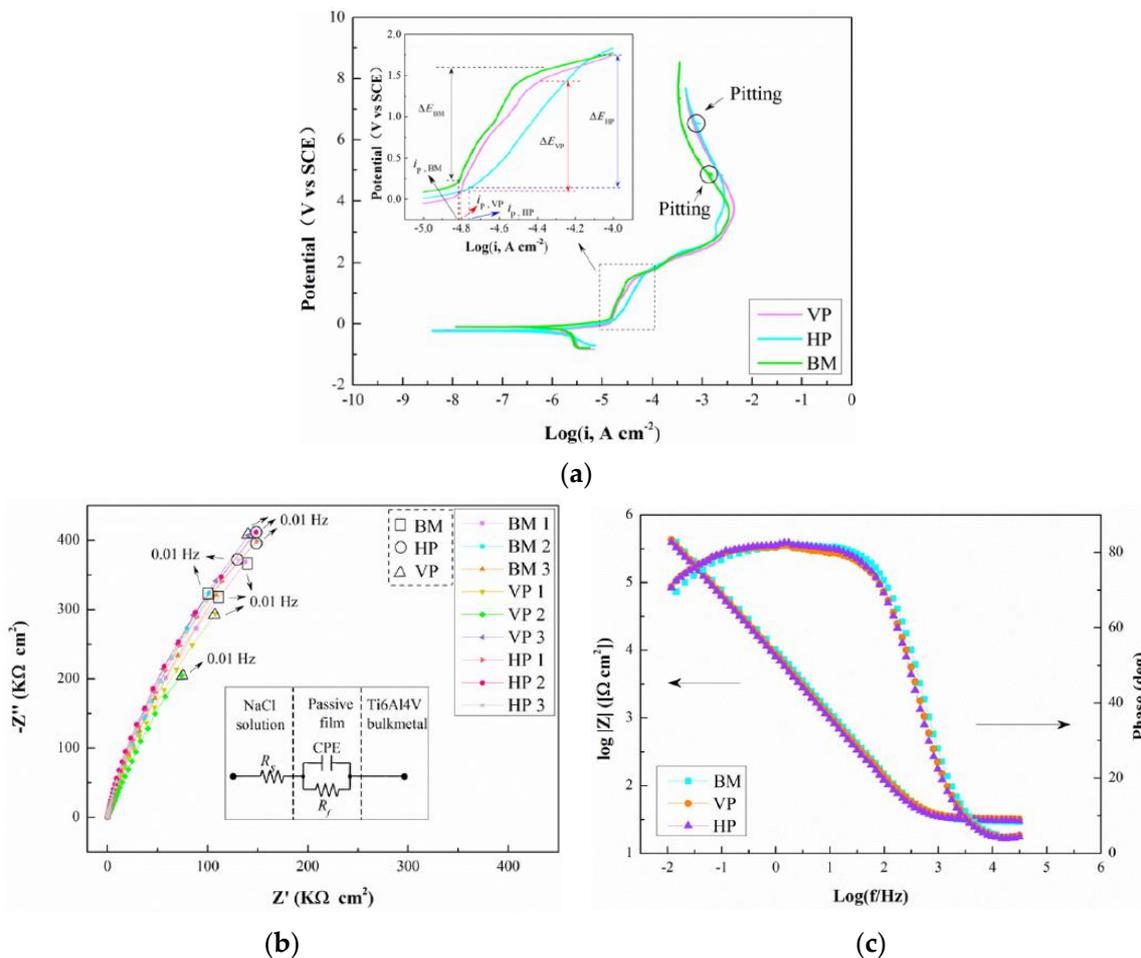
Figure 11. (**a**) Polarisation curves, (**b**) Nyquist plots with EEC, and (**c**) Bode diagrams of WAAMed Ti-6Al-4V. Adapted from [88].
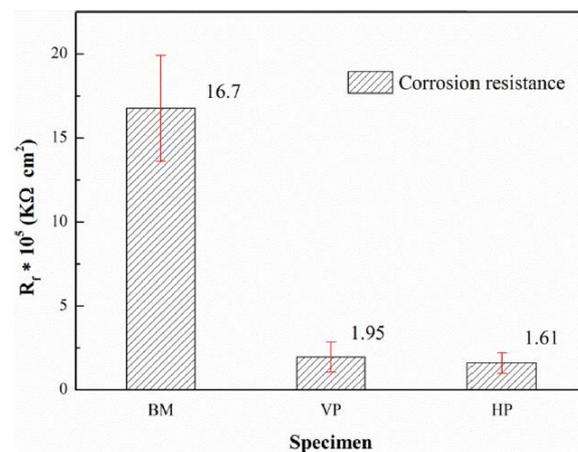
**Figure 12.** The comparison of corrosion resistance of WAAM-fabricated Ti-6Al-4V and wrought base metal in 3.5% NaCl solution. Reprinted with permission from [88].

3.4.2. Magnesium Alloys

Fang et al. investigated the corrosion performance of the WAAMed AZ31 magnesium alloy [89]. In comparison to its hot-rolled counterpart, the WAAMed AZ31 presented lower values of E_{corr}, I_{corr} and corrosion rate in a 3.5% NaCl solution, as observed in Figure 13 and Table 1, indicating an improved corrosion resistance. The authors associated the results with the grain refinement obtained by this AM technique compared to the hot-rolled; approximately 75 μm vs. 1300 μm, respectively, as seen in Figure 14.
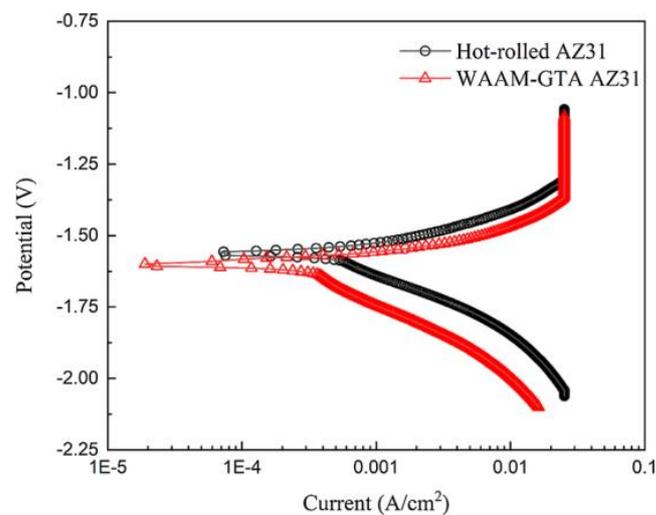
Figure 13. Potentiodynamic polarisation curves of hot-rolled and AMed AZ31 magnesium alloy under 3.5 wt% NaCl solution. Reprinted with permission from [89].

Table 1. Calculated corrosion parameters from the linear polarization curves. Taken from [89].

Sample	I_{corr} (μA/cm^2)	E_{corr} (V)	R_{corr} (mm/year)
Hot-rolled	611.62	−1.56	13.62
WAMMed	154.12	−1.60	3.43
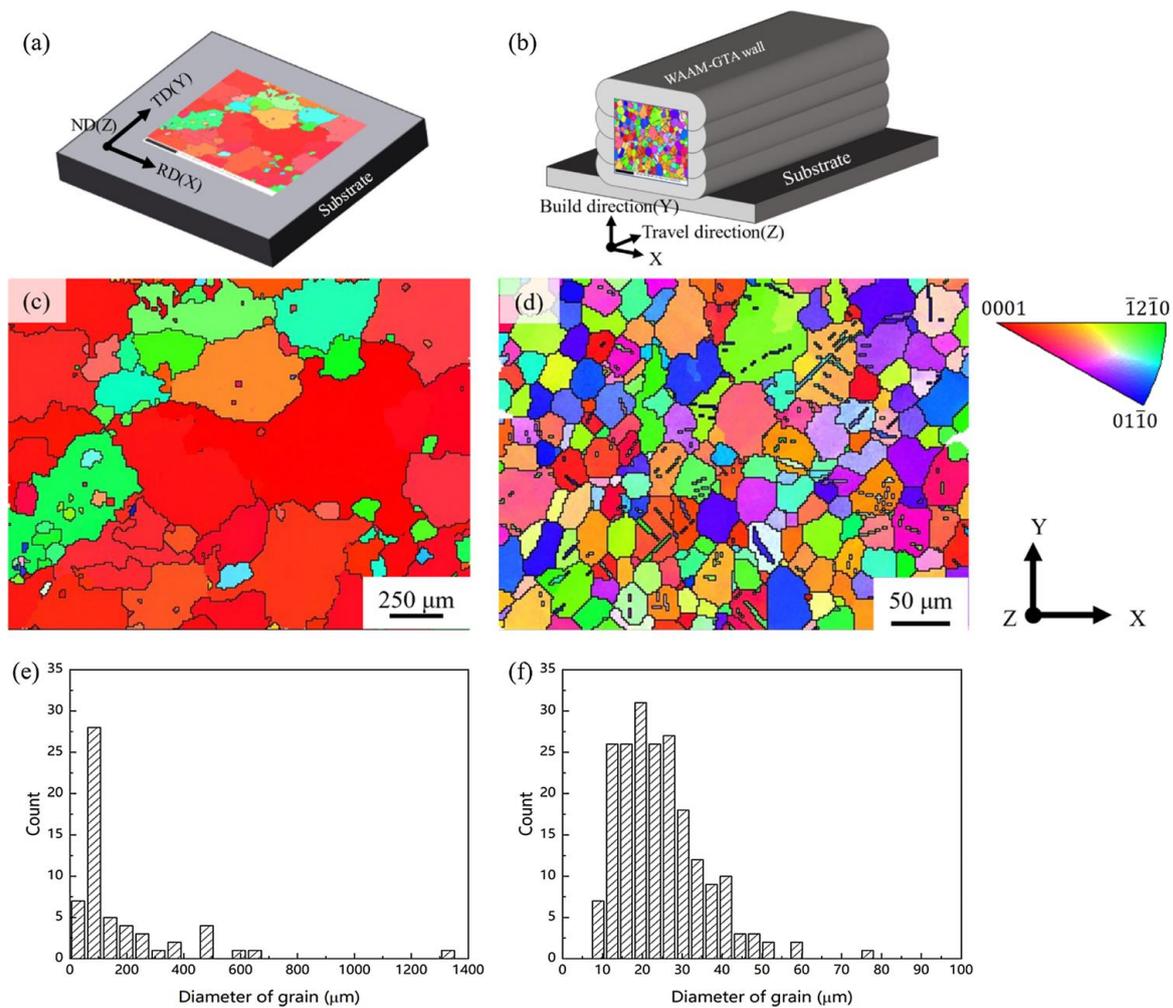
Figure 14. Inverse Pole Figure (IPF) and statistics charts of grain size for the (**a**,**c**,**e**) hot-rolled and (**b**,**d**,**f**) WAAMed AZ31 Mg alloy. Reprinted with permission from [89].

Although the influence of grain size on the corrosion of magnesium alloys is still controversial in the literature, some authors stated that the higher density of grain boundaries facilitates passivation, acting as a corrosion barrier [90–92].

Similarly to Fang et al. [89], Li et al. [93] studied the corrosion behaviour of AZ31 as a function of grain refinement induced by the WAAM process. The main difference between these electrochemical studies was the concentration of the solution. While Fang et al. used 3.5 wt% NaCl, Li et al. used 0.5 wt% NaCl. Under this different condition, it was observed that the WAAMed alloy presented higher i_{corr}, as seen in Figure 15a, and this was associated with the preferential oxidisation of the refined microstructure producing a less protective corrosion products layer. Figure 15b shows that both alloys present filiform corrosion, but the WAAMed alloy differs by presenting intergranular corrosion, which was related to an accelerated dissolution of magnesium surrounding the second phases precipitated along the grain boundaries. This effect was more pronounced in the WAAMed alloy due to the higher density of grain boundaries as a result of the grain refinement.

The analysis of EIS suggests that the cast AZ31 forms a hydroxide layer providing temporary protection for 6 h, while the WAAMed AZ31 does not produce this layer. Figure 15c,d depicts the presence of the layer in the increase in the capacitive loop from 0.5 to 6 h of immersion time, after that the layer is damaged due to Cl^- penetration.
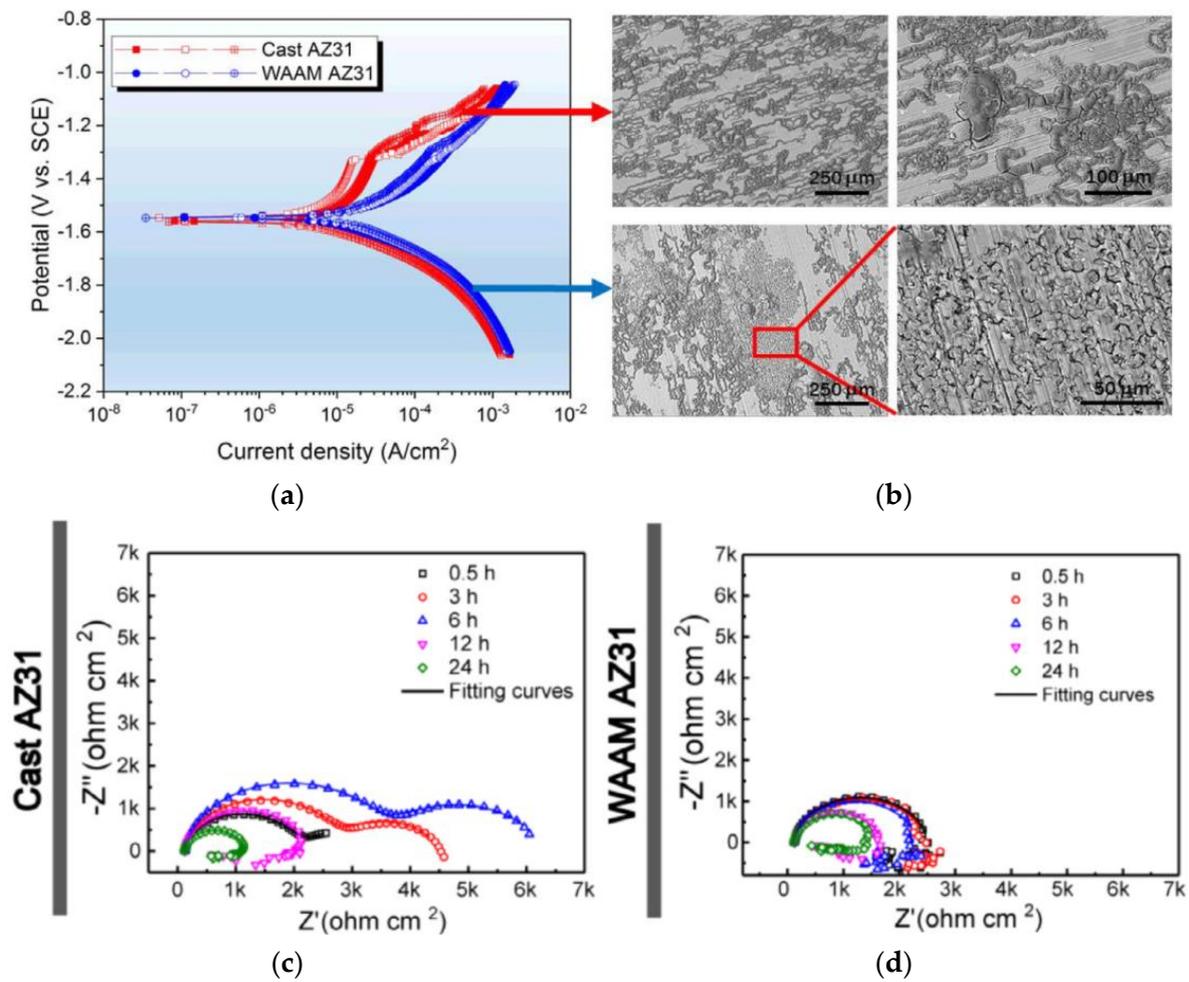
Figure 15. (**a**) Potentiodynamic polarisation curves, (**b**) corresponding surface morphologies of cast AZ31 and WAAM AZ31 immersed in 0.5 wt% NaCl solution with 30 min of stabilisation, (**c**) Nyquist plot of cast AZ31, and (**d**) Nyquist plot of WAAM AZ31 immersed in 0.5 wt% NaCl solution at varied durations. Reprinted with permission from [93].

The authors concluded that hindered corrosion resistance of the WAAMed AZ31 is caused by grain refinement. The corrosion mechanism of the cast alloy with larger grains was micro-galvanic coupling, while intergranular corrosion prevailed over the micro-galvanic corrosion for the significantly reduced grain size of the WAAMed alloy [93].

4. Outlook

Table 2 presents a summary of the effects of the WAAM process on the corrosion susceptibility of the studied alloys. The most common parameter that affected the resistance was the creation of micro-galvanic cells due to solute segregation, emphasising the importance of homogeneous chemical composition within the fabricated material.

Table 2. Summary of the effects of WAAM Process Variables on the Corrosion Susceptibility.

Variables	Effect on Corrosion Susceptibility	WAAM Systems Affected
Solute Segregation	Micro-galvanic cells are created, resulting in localised corrosion [69,77] and different phases along the deposited layer, resulting in distinct corrosion potentials [67].	316LN ER70S-6 10CrNi3MoV

Table 2. *Cont.*

Variables	Effect on Corrosion Susceptibility	WAAM Systems Affected
Refined Grain Size	This variable is still controversial in the literature. Some authors relate coarse and non-equiaxed grains with hindered corrosion behaviour [67,83], while others observe the opposite [77].	10CrNi3MoV 825 alloy TI-6Al-4V
Heat Input	Lower corrosion potentials were observed when applying high heat input [67,69].	10CrNi3MoV 316LN
Current Source	WAAMed materials fabricated using a pulsed current source presented more positive corrosion potentials when compared to constant current sources [72].	SUS 304

5. Future Perspectives and Conclusions

Although WAAM is an emerging AM process for the fabrication of large, complex-shaped structures, most of the existing literature is focused on evaluating the microstructure that develops along the fabricated part, as well as the resulting mechanical (static and cyclic) properties. In opposition, the evaluation of the corrosion behaviour of WAAMed components is still in its infancy, requiring an expansion of dedicated studies to evaluate how the thermal cycle process and microstructure will influence the corrosion behaviour of the fabricated material. The non-equilibrium heating and cooling conditions associated with WAAM render the development of heterogenous microstructures, including compositional gradients that can locally accelerate the material corrosion, enabling premature failure to occur. Different methodologies can be used to understand the corrosion behaviour of WAAMed components, including dedicated tests aimed at revealing how the microstructure influences material degradation in different environments. Moreover, the advent of Integrated Computational Materials Engineering (ICME) approaches [94–98] can enable the development of processing strategies and the selection of different filler materials during WAAM, which can ensure improved and safer corrosion performance of the fabricated components. Moreover, the evaluation of post-processing methodologies, currently widely used for improving the microstructure and mechanical response in fusion-based AMed components [99–105], will need to be further expanded to WAAM in order to determine the most suitable microstructure features for safe operating conditions considering both the mechanical and corrosion performance of the fabricated materials. Thus, the need to develop post-WAAM heat treatment to promote microstructure homogenisation is expected to have a tremendous and positive impact on the corrosion behaviour of WAAMed components. However, WAAM is well-suited for the creation of functionally graded materials [102,106,107], which bring increased complexity for evaluating the corrosion response of the material due to a spatially varying composition and microstructure, while at the same time the post-process heat treatment condition may not be suitable for certain composition ranges within the fabricated functionally graded component. Thus, the need to develop process parameters capable of inducing in situ heat treatments [105,108] that render optimised conditions is expected to be of significant importance for WAAM, while at the same time another possibility may encompass the use of local heat treatments to selectively modify the microstructure of the component. Nonetheless, this last option is likely to be very time-consuming and may render some push back from industries owing to the associated significant time and capital costs for such an approach to be implemented.

The evaluation of stress-induced corrosion is also another key topic that needs to be comprehensively addressed for WAAMed components. Given the potential application of WAAMed components in structural applications where thermomechanical efforts can be expected, the material response under different environments must also be assessed to verify the suitability of this process for application in advanced structural applications. However, as inferred from the current work, this topic is not yet addressed, being a

significant scientific gap in the literature that must be bridged in the near future to enable the full adoption of WAAM for different applications.

To summarise this review work, the following key conclusions can be drawn:

- WAAM is currently being increasingly adopted for the fabrication of complex-shaped metallic structures for structural components.
- The corrosion behaviour of WAAMed structures is currently very limited, which prevents the full evaluation of the potential of this technology for the deployment of metallic structures for application where extreme operating environments are encountered.
- From the still relative number of engineering alloys processed by WAAM for which the corrosion behaviour was evaluated, it was observed that different systems will have a distinct behaviour in a corrosive environment, i.e., while some as-built components outperform wrought counterparts, the opposite is also observed frequently.
- There is a need to precisely determine how local non-equilibrium solidification microstructures, and potentially the effect of post-process heat treatment, will influence the corrosion performance of the component, while at the same time there is a need to evaluate whether the microstructure conditions that render the best corrosion behaviour will also allow the structure to sustain the mechanical efforts for which it was considered.
- The use of ICME methodologies can aid in the development of new materials compositions obtained by WAAM for improved corrosion and mechanical performance for advanced structural applications.

Author Contributions: Writing—original draft preparation, D.A.M.; writing—review and editing, J.P.O. and A.C.B.; supervision, J.P.O. and A.C.B. All authors have read and agreed to the published version of the manuscript.

Conflicts of Interest: The authors declare no conflict of interest.

References

1. Ngo, T.D.; Kashani, A.; Imbalzano, G.; Nguyen, K.T.Q.; Hui, D. Additive Manufacturing (3D Printing): A Review of Materials, Methods, Applications and Challenges. *Compos. B Eng.* **2018**, *143*, 172–196. [CrossRef]
2. Krawiec, P.; Czarnecka-komorowska, D.; Warguła, Ł.; Wojciechowski, S. Geometric Specification of Non-circular Pulleys Made with Various Additive Manufacturing Techniques. *Materials* **2021**, *14*, 1682. [CrossRef] [PubMed]
3. Chandrashekarappa, M.P.G.; Chate, G.R.; Parashivamurthy, V.; Kumar, B.S.; Bandukwala, M.A.N.; Kaisar, A.; Giasin, K.; Pimenov, D.Y.; Wojciechowski, S. Analysis and Optimization of Dimensional Accuracy and Porosity of High Impact Polystyrene Material Printed by FDM Process: PSO, JAYA, Rao, and Bald Eagle Search Algorithms. *Materials* **2021**, *14*, 7479. [CrossRef]
4. Das, S.; Vora, J.J.; Patel, V.; Li, W.; Andersson, J.; Pimenov, D.Y.; Giasin, K.; Wojciechowski, S. Experimental Investigation on Welding of 2.25 Cr-1.0 Mo Steel with Regulated Metal Deposition and GMAW Technique Incorporating Metal-Cored Wires. *J. Mater. Res. Technol.* **2021**, *15*, 1007–1016. [CrossRef]
5. Sheshadri, R.; Nagaraj, M.; Lakshmikanthan, A.; Chandrashekarappa, M.P.G.; Pimenov, D.Y.; Giasin, K.; Prasad, R.V.S.; Wojciechowski, S. Experimental Investigation of Selective Laser Melting Parameters for Higher Surface Quality and Microhardness Properties: Taguchi and Super Ranking Concept Approaches. *J. Mater. Res. Technol.* **2021**, *14*, 2586–2600. [CrossRef]
6. Singh, S.R.; Khanna, P. Wire Arc Additive Manufacturing (WAAM): A New Process to Shape Engineering Materials. *Mater Today Proc.* **2021**, *44*, 118–128. [CrossRef]
7. Cunningham, C.R.; Wikshåland, S.; Xu, F.; Kemakolam, N.; Shokrani, A.; Dhokia, V.; Newman, S.T. Cost Modelling and Sensitivity Analysis of Wire and Arc Additive Manufacturing. *Procedia Manuf.* **2017**, *11*, 650–657. [CrossRef]
8. Le, V.T.; Mai, D.S.; Doan, T.K.; Paris, H. Wire and Arc Additive Manufacturing of 308L Stainless Steel Components: Optimization of Processing Parameters and Material Properties. *Eng. Sci. Technol. Int. J.* **2021**, *24*, 1015–1026. [CrossRef]
9. Hönnige, J.R.; Colegrove, P.A.; Ganguly, S.; Eimer, E.; Kabra, S.; Williams, S. Control of Residual Stress and Distortion in Aluminium Wire + Arc Additive Manufacture with Rolling. *Addit. Manuf.* **2018**, *22*, 775–783. [CrossRef]
10. Li, Y.; Han, Q.; Horváth, I.; Zhang, G. Repairing Surface Defects of Metal Parts by Groove Machining and Wire + Arc Based Filling. *J. Mater. Process. Technol.* **2019**, *274*, 116268. [CrossRef]

11. Xiong, J.; Zhang, G. Online Measurement of Bead Geometry in GMAW-Based Additive Manufacturing Using Passive Vision. *Meas. Sci. Technol.* **2013**, *24*, 115103. [CrossRef]

12. Hu, Z.; Qin, X.; Shao, T.; Liu, H. Understanding and Overcoming of Abnormity at Start and End of the Weld Bead in Additive Manufacturing with GMAW. *Int. J. Adv. Manuf. Technol.* **2018**, *95*, 2357–2368. [CrossRef]

13. Shi, J.; Li, F.; Chen, S.; Zhao, Y.; Tian, H. Effect of In-Process Active Cooling on Forming Quality and Efficiency of Tandem GMAW–Based Additive Manufacturing. *Int. J. Adv. Manuf. Technol.* **2019**, *101*, 1349–1356. [CrossRef]

14. Yang, D.; Wang, G.; Zhang, G. Thermal Analysis for Single-Pass Multi-Layer GMAW Based Additive Manufacturing Using Infrared Thermography. *J. Mater. Process. Technol.* **2017**, *244*, 215–224. [CrossRef]

15. Nilsiam, Y.; Sanders, P.; Pearce, J.M. Slicer and Process Improvements for Open-Source GMAW-Based Metal 3-D Printing. *Addit. Manuf.* **2017**, *18*, 110–120. [CrossRef]

16. Yilmaz, O.; Ugla, A.A. Microstructure Characterization of SS308LSi Components Manufactured by GTAW-Based Additive Manufacturing: Shaped Metal Deposition Using Pulsed Current Arc. *Int. J. Adv. Manuf. Technol.* **2017**, *89*, 13–25. [CrossRef]

17. Geng, H.; Li, J.; Xiong, J.; Lin, X.; Zhang, F. Optimization of Wire Feed for GTAW Based Additive Manufacturing. *J. Mater. Process. Technol.* **2017**, *243*, 40–47. [CrossRef]

18. Ma, Y.; Cuiuri, D.; Hoye, N.; Li, H.; Pan, Z. The Effect of Location on the Microstructure and Mechanical Properties of Titanium Aluminides Produced by Additive Layer Manufacturing Using In-Situ Alloying and Gas Tungsten Arc Welding. *Mater. Sci. Eng. A* **2015**, *631*, 230–240. [CrossRef]

19. Wang, J.F.; Sun, Q.J.; Wang, H.; Liu, J.P.; Feng, J.C. Effect of Location on Microstructure and Mechanical Properties of Additive Layer Manufactured Inconel 625 Using Gas Tungsten Arc Welding. *Mater. Sci. Eng. A* **2016**, *676*, 395–405. [CrossRef]

20. Lin, J.; Lv, Y.; Liu, Y.; Sun, Z.; Wang, K.; Li, Z.; Wu, Y.; Xu, B. Microstructural Evolution and Mechanical Property of Ti-6Al-4V Wall Deposited by Continuous Plasma Arc Additive Manufacturing without Post Heat Treatment. *J. Mech. Behav. Biomed. Mater.* **2017**, *69*, 19–29. [CrossRef]

21. Liu, W.; Jia, C.; Guo, M.; Gao, J.; Wu, C. Compulsively Constricted WAAM with Arc Plasma and Droplets Ejected from a Narrow Space. *Addit. Manuf.* **2019**, *27*, 109–117. [CrossRef]

22. Jhavar, S.; Jain, N.K.; Paul, C.P. Development of Micro-Plasma Transferred Arc (μ-PTA) Wire Deposition Process for Additive Layer Manufacturing Applications. *J. Mater. Process. Technol.* **2014**, *214*, 1102–1110. [CrossRef]

23. Jhavar, S.; Paul, C.P.; Jain, N.K. Micro-Plasma Transferred Arc Additive Manufacturing for Die and Mold Surface Remanufacturing. *JOM* **2016**, *68*, 1801–1809. [CrossRef]

24. Alberti, E.A.; Bueno, B.M.P.; D'Oliveira, A.S.C.M. Additive Manufacturing Using Plasma Transferred Arc. *Int. J. Adv. Manuf. Technol.* **2016**, *83*, 1861–1871. [CrossRef]

25. Ayarkwa, K.F.; Williams, S.W.; Ding, J. Assessing the Effect of TIG Alternating Current Time Cycle on Aluminium Wire + Arc Additive Manufacture. *Addit. Manuf.* **2017**, *18*, 186–193. [CrossRef]

26. Yin, B.; Ma, H.; Wang, J.; Fang, K.; Zhao, H.; Liu, Y. Effect of CaF_2 Addition on Macro/Microstructures and Mechanical Properties of Wire and Arc Additive Manufactured Ti-6Al-4V Components. *Mater. Lett.* **2017**, *190*, 64–66. [CrossRef]

27. Oyama, K.; Diplas, S.; M'hamdi, M.; Gunnæs, A.E.; Azar, A.S. Heat Source Management in Wire-Arc Additive Manufacturing Process for Al-Mg and Al-Si Alloys. *Addit. Manuf.* **2019**, *26*, 180–192. [CrossRef]

28. Wang, L.; Suo, Y.; Liang, Z.; Wang, D.; Wang, Q. Effect of Titanium Powder on Microstructure and Mechanical Properties of Wire + arc Additively Manufactured Al-Mg Alloy. *Mater. Lett.* **2019**, *241*, 231–234. [CrossRef]

29. Ding, D.; Pan, Z.; Cuiuri, D.; Li, H. A Practical Path Planning Methodology for Wire and Arc Additive Manufacturing of Thin-Walled Structures. *Robot. Comput. Integr. Manuf.* **2015**, *34*, 8–19. [CrossRef]

30. Li, F.; Chen, S.; Shi, J.; Zhao, Y.; Tian, H. Thermoelectric Cooling-Aided Bead Geometry Regulation in Wire and Arc-Based Additive Manufacturing of Thin-Walled Structures. *Appl. Sci.* **2018**, *8*, 207. [CrossRef]

31. Gu, J.; Wang, X.; Bai, J.; Ding, J.; Williams, S.; Zhai, Y.; Liu, K. Deformation Microstructures and Strengthening Mechanisms for the Wire+arc Additively Manufactured Al-Mg4.5Mn Alloy with Inter-Layer Rolling. *Mater. Sci. Eng. A* **2018**, *712*, 292–301. [CrossRef]

32. Dirisu, P.; Ganguly, S.; Mehmanparast, A.; Martina, F.; Williams, S. Analysis of Fracture Toughness Properties of Wire + Arc Additive Manufactured High Strength Low Alloy Structural Steel Components. *Mater. Sci. Eng. A* **2019**, *765*, 138285. [CrossRef]

33. Dowson, D.; Neville, A. Tribology and Corrosion in Hip Joint Replacements: Materials and Engineering. In *Joint Replacement Technology*; Woodhead Publishing: Cambridge, UK, 2014; pp. 401–442.

34. Dai, C.; Fu, Y.; Guo, J.; Du, C. Effects of Substrate Temperature and Deposition Time on the Morphology and Corrosion Resistance of FeCoCrNiMo0.3 High-Entropy Alloy Coating Fabricated by Magnetron Sputtering. *Int. J. Miner. Metall. Mater.* **2020**, *27*, 1388–1397. [CrossRef]

35. Tayyab, K.B.; Farooq, A.; Alvi, A.A.; Nadeem, A.B.; Deen, K.M. Corrosion Behavior of Cold-Rolled and Post Heat-Treated 316L Stainless Steel in 0.9wt% NaCl Solution. *Int. J. Miner. Metall. Mater.* **2021**, *28*, 440–449. [CrossRef]

36. Aldalur, E.; Veiga, F.; Suárez, A.; Bilbao, J.; Lamikiz, A. High Deposition Wire Arc Additive Manufacturing of Mild Steel: Strategies and Heat Input Effect on Microstructure and Mechanical Properties. *J. Manuf. Process.* **2020**, *58*, 615–626. [CrossRef]

37. Su, C.; Chen, X.; Gao, C.; Wang, Y. Effect of Heat Input on Microstructure and Mechanical Properties of Al-Mg Alloys Fabricated by WAAM. *Appl. Surf. Sci.* **2019**, *486*, 431–440. [CrossRef]

38. Dinovitzer, M.; Chen, X.; Laliberte, J.; Huang, X.; Frei, H. Effect of Wire and Arc Additive Manufacturing (WAAM) Process Parameters on Bead Geometry and Microstructure. *Addit. Manuf.* **2019**, *26*, 138–146. [CrossRef]

39. Klein, T.; Schnall, M. Control of Macro-/Microstructure and Mechanical Properties of a Wire-Arc Additive Manufactured Aluminum Alloy. *Int. J. Adv. Manuf. Technol.* **2020**, *108*, 235–244. [CrossRef]
40. MacDonald, E.; Wicker, R. Multiprocess 3D Printing for Increasing Component Functionality. *Science (1979)* **2016**, *353*, aaf2093. [CrossRef] [PubMed]
41. Selvi, S.; Vishvaksenan, A.; Rajasekar, E. Cold Metal Transfer (CMT) Technology—An Overview. *Def. Technol.* **2018**, *14*, 28–44. [CrossRef]
42. Chen, S.; Tong, Y.; Liaw, P. Additive Manufacturing of High-Entropy Alloys: A Review. *Entropy* **2018**, *20*, 937. [CrossRef] [PubMed]
43. Everton, S.K.; Hirsch, M.; Stravroulakis, P.; Leach, R.K.; Clare, A.T. Review of In-Situ Process Monitoring and in-Situ Metrology for Metal Additive Manufacturing. *Mater. Des.* **2016**, *95*, 431–445. [CrossRef]
44. Beese, A.M.; Carroll, B.E. Review of Mechanical Properties of Ti-6Al-4V Made by Laser-Based Additive Manufacturing Using Powder Feedstock. *JOM* **2016**, *68*, 724–734. [CrossRef]
45. Khorasani, A.; Gibson, I.; Veetil, J.K.; Ghasemi, A.H. A Review of Technological Improvements in Laser-Based Powder Bed Fusion of Metal Printers. *Int. J. Adv. Manuf. Technol.* **2020**, *108*, 191–209. [CrossRef]
46. Frazier, W.E. Metal Additive Manufacturing: A Review. *J. Mater. Eng. Perform.* **2014**, *23*, 1917–1928. [CrossRef]
47. Huang, S.H.; Liu, P.; Mokasdar, A.; Hou, L. Additive Manufacturing and Its Societal Impact: A Literature Review. *Int. J. Adv. Manuf. Technol.* **2013**, *67*, 1191–1203. [CrossRef]
48. Bandyopadhyay, A.; Heer, B. Additive Manufacturing of Multi-Material Structures. *Mater. Sci. Eng. R Rep.* **2018**, *129*, 1–16. [CrossRef]
49. Haghdadi, N.; Laleh, M.; Moyle, M.; Primig, S. Additive Manufacturing of Steels: A Review of Achievements and Challenges. *J. Mater. Sci.* **2021**, *56*, 64–107. [CrossRef]
50. Xu, F.; Luo, L.; Xiong, L.; Liu, Y. Microstructure and Corrosion Behavior of ALD Al2O3 Film on AZ31 Magnesium Alloy with Different Surface Roughness. *J. Magnes. Alloys* **2020**, *8*, 480–492. [CrossRef]
51. Sasaki, K.; Burstein, G.T. The Generation of Surface Roughness during Slurry Erosion-Corrosion and Its Effect on the Pitting Potential. *Corros. Sci.* **1996**, *38*, 2111–2120. [CrossRef]
52. Zhang, X.; Lv, Y.; Tan, S.; Dong, Z.; Zhou, X. Microstructure and Corrosion Behaviour of Wire Arc Additive Manufactured AA2024 Alloy Thin Wall Structure. *Corros. Sci.* **2021**, *186*, 109453. [CrossRef]
53. Bajaj, P.; Hariharan, A.; Kini, A.; Kürnsteiner, P.; Raabe, D.; Jägle, E.A. Steels in Additive Manufacturing: A Review of Their Microstructure and Properties. *Mater. Sci. Eng. A* **2020**, *772*, 138633. [CrossRef]
54. Sander, G.; Tan, J.; Balan, P.; Gharbi, O.; Feenstra, D.R.; Singer, L.; Thomas, S.; Kelly, R.G.; Scully, J.R.; Birbilis, N. Corrosion of Additively Manufactured Alloys: A Review. *Corrosion* **2018**, *74*, 1318–1350. [CrossRef] [PubMed]
55. Raut, L.P.; Taiwade, R. v Wire Arc Additive Manufacturing: A Comprehensive Review and Research Directions. *J. Mater. Eng. Perform.* **2021**, *30*, 4768–4791. [CrossRef]
56. Ko, G.; Kim, W.; Kwon, K.; Lee, T.-K. The Corrosion of Stainless Steel Made by Additive Manufacturing: A Review. *Metals* **2021**, *11*, 516. [CrossRef]
57. Available online: https://Www.Sciencedirect.Com (accessed on 24 January 2023).
58. Ahsan, M.R.U.; Seo, G.-J.; Fan, X.; Liaw, P.K.; Motaman, S.; Haase, C.; Kim, D.B. Effects of Process Parameters on Bead Shape, Microstructure, and Mechanical Properties in Wire + Arc Additive Manufacturing of Al0.1CoCrFeNi High-Entropy Alloy. *J. Manuf. Process.* **2021**, *68*, 1314–1327. [CrossRef]
59. Wu, B.; Pan, Z.; Ding, D.; Cuiuri, D.; Li, H. Effects of Heat Accumulation on Microstructure and Mechanical Properties of Ti6Al4V Alloy Deposited by Wire Arc Additive Manufacturing. *Addit. Manuf.* **2018**, *23*, 151–160. [CrossRef]
60. Qi, Z.; Cong, B.; Qi, B.; Zhao, G.; Ding, J. Properties of Wire + arc Additively Manufactured 2024 Aluminum Alloy with Different Solution Treatment Temperature. *Mater. Lett.* **2018**, *230*, 275–278. [CrossRef]
61. Wu, B.; Pan, Z.; Ding, D.; Cuiuri, D.; Li, H.; Fei, Z. The Effects of Forced Interpass Cooling on the Material Properties of Wire Arc Additively Manufactured Ti6Al4V Alloy. *J. Mater. Process. Technol.* **2018**, *258*, 97–105. [CrossRef]
62. Guo, J.; Zhou, Y.; Liu, C.; Wu, Q.; Chen, X.; Lu, J. Wire Arc Additive Manufacturing of AZ31 Magnesium Alloy: Grain Refinement by Adjusting Pulse Frequency. *Materials* **2016**, *9*, 823. [CrossRef]
63. Donoghue, J.; Antonysamy, A.A.; Martina, F.; Colegrove, P.A.; Williams, S.W.; Prangnell, P.B. The Effectiveness of Combining Rolling Deformation with Wire–Arc Additive Manufacture on β-Grain Refinement and Texture Modification in Ti–6Al–4V. *Mater. Charact.* **2016**, *114*, 103–114. [CrossRef]
64. Osintsev, K.; Konovalov, S.; Zaguliaev, D.; Ivanov, Y.; Gromov, V.; Panchenko, I. Investigation of Co-Cr-Fe-Mn-Ni Non-Equiatomic High-Entropy Alloy Fabricated by Wire Arc Additive Manufacturing. *Metals* **2022**, *12*, 197. [CrossRef]
65. Wu, B.; Pan, Z.; Ding, D.; Cuiuri, D.; Li, H.; Xu, J.; Norrish, J. A Review of the Wire Arc Additive Manufacturing of Metals: Properties, Defects and Quality Improvement. *J. Manuf. Process.* **2018**, *35*, 127–139. [CrossRef]
66. Chen, W.; Chen, Y.; Zhang, T.; Wen, T.; Yin, Z.; Feng, X. Effect of Ultrasonic Vibration and Interpass Temperature on Microstructure and Mechanical Properties of Cu-8Al-2Ni-2Fe-2Mn Alloy Fabricated by Wire Arc Additive Manufacturing. *Metals* **2020**, *10*, 215. [CrossRef]
67. Tian, G.; Wang, X.; Wang, W.; Chang, Q.; Zhao, Y.; Han, G.; Ren, Z.; Zhu, S. Microstructure, Mechanical Properties, and Galvanic Corrosion of 10CrNi3MoV Fabricated by Wire Arc Additive Manufacturing. *Metals* **2021**, *11*, 1235. [CrossRef]

68. Ron, T.; Levy, G.K.; Dolev, O.; Leon, A.; Shirizly, A.; Aghion, E. Environmental Behavior of Low Carbon Steel Produced by a Wire Arc Additive Manufacturing Process. *Metals* **2019**, *9*, 888. [CrossRef]

69. Wen, D.; Long, P.; Li, J.; Huang, L.; Zheng, Z. Effects of Linear Heat Input on Microstructure and Corrosion Behavior of an Austenitic Stainless Steel Processed by Wire Arc Additive Manufacturing. *Vacuum* **2020**, *173*, 109131. [CrossRef]

70. Jegdić, B.; Bobić, B.; Radojković, B.; Alić, B.; Radovanović, L. Corrosion Resistance of Welded Joints of X5CrNi18-10 Stainless Steel. *J. Mater. Process. Technol.* **2019**, *266*, 579–587. [CrossRef]

71. Paulraj, P.; Garg, R. Effect of Welding Parameters on Pitting Behavior of GTAW of DSS and Super DSS Weldments. *Eng. Sci. Technol. Int. J.* **2016**, *19*, 1076–1083. [CrossRef]

72. Hao, Z.; Ao, S.; Cai, Y.; Zhang, W.; Luo, Z. Formation of SUS304/Aluminum Alloys Using Wire and Arc Additive Manufacturing. *Metals* **2018**, *8*, 595. [CrossRef]

73. Rajesh Kannan, A.; Siva Shanmugam, N.; Rajkumar, V.; Vishnukumar, M. Insight into the Microstructural Features and Corrosion Properties of Wire Arc Additive Manufactured Super Duplex Stainless Steel (ER2594). *Mater. Lett.* **2020**, *270*, 127680. [CrossRef]

74. Fontana, M.G.; Greene, N.D. *Corrosion Engineering*, 3rd ed.; McGraw-Hill: New York, NY, USA, 1985.

75. *ANSI/NACE MR0175/ISO 15156-1:2015*; Petroleum, Petrochemical, and Natural Gas Industries-Materials for Use in H_2S-Containing Environments in Oil and Gas Production-Part 1: General Principles for Selection of Cracking-Resistant Materials. NACE International: Houston, TX, USA, 2015.

76. *NORSOK M-630 NORSOK STANDARD Material Data Sheets and Element Data Sheets for Piping*, 7th ed.; Norwegian Technology Centre: Oslo, Norway, 2020.

77. Zhang, L.N.; Ojo, O.A. Corrosion Behavior of Wire Arc Additive Manufactured Inconel 718 Superalloy. *J. Alloys Compd.* **2020**, *829*, 154455. [CrossRef]

78. Guo, P.; Lin, X.; Li, J.; Zhang, Y.; Song, M.; Huang, W. Electrochemical Behavior of Inconel 718 Fabricated by Laser Solid Forming on Different Sections. *Corros. Sci.* **2018**, *132*, 79–89. [CrossRef]

79. Chigilipalli, B.K.; Veeramani, A. Investigation of the Corrosion Behavior of Wire Arc Additively Manufactured Alloy 825. *Trans. Indian Inst. Met.* **2022**, *76*, 279–286. [CrossRef]

80. Babu, K.T.; Muthukumaran, S.; Kumar, C.H.B.; Narayanan, C.S. Improvement in Mechanical and Metallurgical Properties of Friction Stir Welded 6061-T6 Aluminum Alloys through Cryogenic Treatment. *Mater. Sci. Forum* **2019**, *969*, 490–495. [CrossRef]

81. Guo, C.; Ying, M.; Dang, H.; Hu, R.; Chen, F. Microstructural and Intergranular Corrosion Properties of Inconel 625 Superalloys Fabricated Using Wire Arc Additive Manufacturing. *Mater. Res. Express* **2021**, *8*, 035103. [CrossRef]

82. Saikiran, A.; Hariprasad, S.; Arun, S.; Rama Krishna, L.; Rameshbabu, N. Effect of Electrolyte Composition on Morphology and Corrosion Resistance of Plasma Electrolytic Oxidation Coatings on Aluminized Steel. *Surf. Coat. Technol.* **2019**, *372*, 239–251. [CrossRef]

83. Yang, J.; Yang, H.; Yu, H.; Wang, Z.; Zeng, X. Corrosion Behavior of Additive Manufactured Ti-6Al-4V Alloy in NaCl Solution. *Metall. Mater. Trans. A* **2017**, *48*, 3583–3593. [CrossRef]

84. *ASTM G102-89(2015)E1*; Standard Practice for Calculation of Corrosion Rates and Related Information from Electrochemical Measurements. ASTM: West Conshohocken, PA, USA, 2015; Volume 89.

85. Chelariu, R.; Bolat, G.; Izquierdo, J.; Mareci, D.; Gordin, D.M.; Gloriant, T.; Souto, R.M. Metastable Beta Ti-Nb-Mo Alloys with Improved Corrosion Resistance in Saline Solution. *Electrochim. Acta* **2014**, *137*, 280–289. [CrossRef]

86. Bolat, G.; Mareci, D.; Chelariu, R.; Izquierdo, J.; González, S.; Souto, R.M. Investigation of the Electrochemical Behaviour of TiMo Alloys in Simulated Physiological Solutions. *Electrochim. Acta* **2013**, *113*, 470–480. [CrossRef]

87. Pan, C.; Wang, X.; Behnamian, Y.; Wu, Z.; Qin, Z.; Xia, D.-H.; Hu, W. Monododecyl Phosphate Film on LY12 Aluminum Alloy: PH-Controlled Self-Assembly and Corrosion Resistance. *J. Electrochem. Soc.* **2020**, *167*, 161510. [CrossRef]

88. Wu, B.; Pan, Z.; Li, S.; Cuiuri, D.; Ding, D.; Li, H. The Anisotropic Corrosion Behaviour of Wire Arc Additive Manufactured Ti-6Al-4V Alloy in 3.5% NaCl Solution. *Corros. Sci.* **2018**, *137*, 176–183. [CrossRef]

89. Fang, X.; Yang, J.; Wang, S.; Wang, C.; Huang, K.; Li, H.; Lu, B. Additive Manufacturing of High Performance AZ31 Magnesium Alloy with Full Equiaxed Grains: Microstructure, Mechanical Property, and Electromechanical Corrosion Performance. *J. Mater. Process. Technol.* **2022**, *300*, 117430. [CrossRef]

90. Alvarez-Lopez, M.; Pereda, M.D.; del Valle, J.A.; Fernandez-Lorenzo, M.; Garcia-Alonso, M.C.; Ruano, O.A.; Escudero, M.L. Corrosion Behaviour of AZ31 Magnesium Alloy with Different Grain Sizes in Simulated Biological Fluids☆. *Acta Biomater.* **2010**, *6*, 1763–1771. [CrossRef]

91. Zhang, T.; Shao, Y.; Meng, G.; Cui, Z.; Wang, F. Corrosion of Hot Extrusion AZ91 Magnesium Alloy: I-Relation between the Microstructure and Corrosion Behavior. *Corros. Sci.* **2011**, *53*, 1960–1968. [CrossRef]

92. Argade, G.R.; Panigrahi, S.K.; Mishra, R.S. Effects of Grain Size on the Corrosion Resistance of Wrought Magnesium Alloys Containing Neodymium. *Corros. Sci.* **2012**, *58*, 145–151. [CrossRef]

93. LI, J.; Qiu, Y.; Yang, J.; Sheng, Y.; Yi, Y.; Zeng, X.; Chen, L.; Yin, F.; Su, J.; Zhang, T.; et al. Effect of Grain Refinement Induced by Wire and Arc Additive Manufacture (WAAM) on the Corrosion Behaviors of AZ31 Magnesium Alloy in NaCl Solution. *J. Magnes. Alloys* **2021**, *11*, 217–229. [CrossRef]

94. Walbrühl, M.; Linder, D.; Ågren, J.; Borgenstam, A. Modelling of Solid Solution Strengthening in Multicomponent Alloys. *Mater. Sci. Eng. A* **2017**, *700*, 301–311. [CrossRef]

95. Wang, X.; Xiong, W. Uncertainty Quantification and Composition Optimization for Alloy Additive Manufacturing through a CALPHAD-Based ICME Framework. *NPJ Comput. Mater.* **2020**, *6*, 188. [CrossRef]

96. Motaman, S.A.H.; Kies, F.; Köhnen, P.; Létang, M.; Lin, M.; Molotnikov, A.; Haase, C. Optimal Design for Metal Additive Manufacturing: An Integrated Computational Materials Engineering (ICME) Approach. *JOM* **2020**, *72*, 1092–1104. [CrossRef]

97. Pires, P.-A.; Desmaison, O.; Megahed, M. ICME Manufacturability Assessment in Powder Bed Fusion Additive Manufacturing. *JOM* **2018**, *70*, 1677–1685. [CrossRef]

98. Seifi, M.; Salem, A.; Beuth, J.; Harrysson, O.; Lewandowski, J.J. Overview of Materials Qualification Needs for Metal Additive Manufacturing. *JOM* **2016**, *68*, 747–764. [CrossRef]

99. Ali, H.; Ghadbeigi, H.; Mumtaz, K. Effect of Scanning Strategies on Residual Stress and Mechanical Properties of Selective Laser Melted Ti6Al4V. *Mater. Sci. Eng. A* **2018**, *712*, 175–187. [CrossRef]

100. Vrancken, B.; Thijs, L.; Kruth, J.-P.; Van Humbeeck, J. Heat Treatment of Ti6Al4V Produced by Selective Laser Melting: Microstructure and Mechanical Properties. *J. Alloys Compd.* **2012**, *541*, 177–185. [CrossRef]

101. Aboulkhair, N.T.; Everitt, N.M.; Ashcroft, I.; Tuck, C. Reducing Porosity in AlSi10Mg Parts Processed by Selective Laser Melting. *Addit. Manuf.* **2014**, *1–4*, 77–86. [CrossRef]

102. Shen, C.; Pan, Z.; Ding, D.; Yuan, L.; Nie, N.; Wang, Y.; Luo, D.; Cuiuri, D.; van Duin, S.; Li, H. The Influence of Post-Production Heat Treatment on the Multi-Directional Properties of Nickel-Aluminum Bronze Alloy Fabricated Using Wire-Arc Additive Manufacturing Process. *Addit. Manuf.* **2018**, *23*, 411–421. [CrossRef]

103. Yang, Y.; Hu, J.; Liu, X.Y.; Xu, W.; Li, B.; Ling, G.P.; Pang, X.Y.; Tian, Y.Z. Post Treatment of an Additively Manufactured Composite Consisting of 304L Stainless Steel and CoCrFeMnNi High-Entropy Alloy. *Mater. Sci. Eng. A* **2022**, *831*, 142104. [CrossRef]

104. Wolcott, P.J.; Hehr, A.; Pawlowski, C.; Dapino, M.J. Process Improvements and Characterization of Ultrasonic Additive Manufactured Structures. *J. Mater. Process. Technol.* **2016**, *233*, 44–52. [CrossRef]

105. Sames, W.J.; Unocic, K.A.; Helmreich, G.W.; Kirka, M.M.; Medina, F.; Dehoff, R.R.; Babu, S.S. Feasibility of in Situ Controlled Heat Treatment (ISHT) of Inconel 718 during Electron Beam Melting Additive Manufacturing. *Addit. Manuf.* **2017**, *13*, 156–165. [CrossRef]

106. Shen, C.; Pan, Z.; Cuiuri, D.; Roberts, J.; Li, H. Fabrication of Fe-FeAl Functionally Graded Material Using the Wire-Arc Additive Manufacturing Process. *Metall. Mater. Trans. B* **2016**, *47*, 763–772. [CrossRef]

107. Shen, Q.; Kong, X.; Chen, X. Fabrication of Bulk Al-Co-Cr-Fe-Ni High-Entropy Alloy Using Combined Cable Wire Arc Additive Manufacturing (CCW-AAM): Microstructure and Mechanical Properties. *J. Mater. Sci. Technol.* **2021**, *74*, 136–142. [CrossRef]

108. Kim, Y.-K.; Baek, M.-S.; Yang, S.; Lee, K.-A. In-Situ Formed Oxide Enables Extraordinary High-Cycle Fatigue Resistance in Additively Manufactured CoCrFeMnNi High-Entropy Alloy. *Addit. Manuf.* **2021**, *38*, 101832. [CrossRef]